Indian J Phys (May 2017) 91(5):547–554
DOI 10.1007/s12648-016-0950-6

ORIGINAL PAPER

Swift heavy ion induced optical and structural modifications in RF sputtered nanocrystalline ZnO thin film

S K Singh[1], R Singhal[1]*, R Vishnoi[1], V V S Kumar[2] and P K Kulariya[2]

[1]Department of Physics, Malaviya National Institute of Technology Jaipur, JLN Marg, Malaviya Nagar, Jaipur 302017, India

[2]Inter University Accelerator Centre, Aruna Asaf Ali Marg, New Delhi 110067, India

Received: 01 November 2016 / Accepted: 23 December 2016 / Published online: 13 January 2017

Abstract: In the present study, 100 MeV Ag^{7+} ion beam-induced structural and optical modifications of nanocrystalline ZnO thin films are investigated. The nanocrystalline ZnO thin films are grown using radio frequency magnetron sputtering and irradiated at fluences of 3×10^{12}, 1×10^{13} and 3×10^{13} ions/cm^2. The incident swift heavy ions induced change in the crystallinity together with the preferential growth of crystallite size along the *c* axis (002) orientation. The average crystallite size is found to be increased from 10.8 ± 0.7 to 20.5 ± 0.3 nm with increasing the ion fluence. The Atomic force microscopy analysis confirms the variation in the surface roughness by varying the incident ion fluences. The UV–visible spectroscopy shows the decrement in transmittance of the film with ion irradiation. The micro-Raman spectra of ZnO thin films are investigated to observe ion-induced modifications which support the increased lattice defects with higher fluence. The variation in crystallinity indicates that ZnO-based devices can be used in piezoelectric transduction mechanism.

Keywords: ZnO thin film; Swift heavy ions; Atomic force microscopy; X-ray diffraction

PACS Nos.: 77.55.hf; 96.50.Vg; 68.37.Ps

1. Introduction

The oxide semiconductors possess various physical properties such as transparency, conductivity, and piezoelectricity which makes them of great scientific interest for optoelectronic and piezoelectric device applications. Among all, ZnO (*n*-type) semiconductor is a very promising material of II–VI group due to its wide band gap ~3.35 eV and large exciton binding energy of 60 meV [1, 2]. The larger band gap of ZnO in comparison to Si and Ge makes it more favourable to use at high temperature in electronic devices. The physical properties of ZnO are widely influenced by deposition conditions and parameters. To analyze the effects of deposition on film properties, many techniques such as sol–gel method, spray pyrolysis, metal organic chemical vapour deposition, pulse laser deposition and RF/DC sputtering have been used and reported by many groups [3–7]. Due to its functionalize properties, ZnO is used in solar cells, transparent conductive contacts, gas sensors, thin film transistors and laser diodes [8–13]. The variability of piezoelectric properties of ZnO, make it useful also for short-wavelength light emitting diodes, optical waveguides, laser deflectors and surface acoustic wave (SAW) band-pass filters [14–16].

Nowadays, researchers are trying to improve the properties of different materials using swift heavy ion (SHI) irradiation. Ion irradiation is a precise technique to modify optical, structural and electrical properties of materials in the nanometer region due to its spatial selectivity [17–28]. Ion beam technique is more advantageous in comparison to other methods because of good control of incident ion energy and fluence. As the swift heavy ions (SHI) traverse through the target material, it interacts with material by losing their energy in two different way; (a) direct transfer of energy to target atoms by elastic collisions, termed as nuclear energy loss (S_n) and (b) transfer of energy of incoming ions to the electrons of target atoms, termed as electronic energy loss (S_e). This energy transfer leads to the

*Corresponding author, E-mail: rahuliuac@gmail.com; rsinghal.-phy@mnit.ac.in

atomic displacement in a cylindrical zone around the incident ion path of material which is explained by two established models; Coulomb spike model (CSM) and Thermal spike model (TSM). According to the CSM, a passage of high energy ions through a material produces ionized cylindrical zone for the time duration of $\sim 10^{-17}$ s. This cylindrical zone contains higher charge region which leads to electrostatic repulsion between incident ions and target atoms and responsible for coherent radial atomic movements under Coulomb force. On the other hand, in Thermal spike model, the incident ion transfers its energy to the electronic subsystem via electron–phonon coupling (EPC) which leads to the rapidly rise in the lattice temperature of the materials above its melting point. Due to the energy dissipation by the thermal conduction, rapid quenching process takes place. This process is responsible for the modifications in the cylindrical zone around the ion path [29, 30]. Schematic diagram for ion–matter interaction is shown in Fig. 1.

The high energy ion beam has been proved very efficient tool to alter the properties of ZnO thin films. The energetic ions loss their energy after interaction with ZnO thin film and transfer excess amount of energy, which creates the density of defects, stress, and strain in the structure of ZnO. The formation of self-affine nanostructure over the surface of ZnO thin films using SHI has been investigated by Agarwal et al. [31]. They reported that the shape and density of these nanostructures depend on incident ion fluence. The effect of 120 MeV Au ion beam on ZnO thin films prepared by the sol–gel method has been investigated by Singh et al. [32] and it was observed that SHI irradiation induced disorder and high density of lattice defects causes to evolution of A_1 (LO) mode. The energetic ions can also be used for better understanding of phonon modes in nanostructures. The structural and spectroscopic modifications of nanocrystalline ZnO thin films using 120 MeV Au ion beam have been analysed by Rehman et al. [33]. They found that nanocrystals become more oriented at low fluences however at higher fluences, the release of strain and decrease in grain size was observed. These modifications could be used in radiation harsh environment for optoelectronic applications.

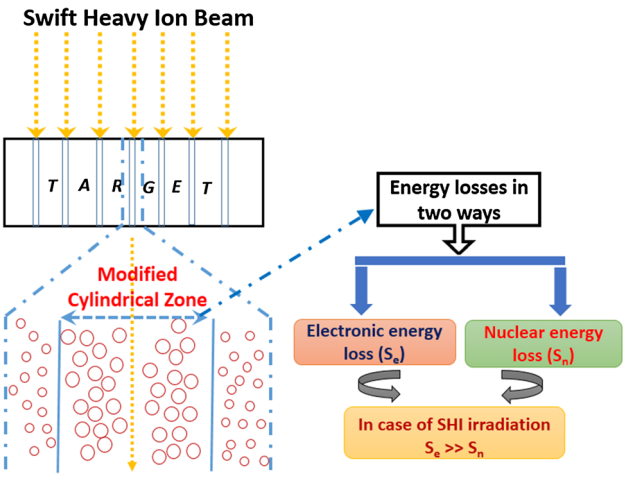

Fig. 1 Schematics diagram for ion–matter interaction

In present work, the structural, optical, and morphological modifications in ZnO thin film induced by 100 MeV Ag^{7+} ions have been investigated. The modifications have been analyzed using different characterization techniques such as X-ray diffraction (XRD), UV–visible spectroscopy, Atomic force microscopy (AFM), Raman spectroscopy and Scanning electron microscopy (SEM). All the modifications induced by energetic ions may be favourable in device fabrication.

2. Experimental details

The sputtering target of pure ZnO was prepared with ZnO powder (99.99%, Alfa-Aesar) by using a hydraulic press machine (HYCON Hydraulic engineers and consultants, New Delhi) with pressure approximately ~ 7 ton. The prepared target was sintered for 24 h at the temperature 1200 °C by sequential steps in a programmable furnace with a continuous flow of oxygen gas. Thin films of ZnO were deposited on glass and silicon substrates at room temperature by radio-frequency (RF) magnetron sputtering, using ZnO target of 2-inch diameter and 3 mm thickness in the presence of Ar environment (grade-I with flow rate ~ 4 sccm). A base pressure of $\sim 10^{-6}$ mbar was achieved by using a turbo-molecular pump before deposition. The sputtering was carried out at a pressure of $\sim 5 \times 10^{-2}$ mbar with a target to substrate distance of 40 mm. The deposition was performed for 15 min at fixed RF power 150 watts, and self-bias voltage 250–280 V. For the film deposition, substrates were cleaned in an ultrasonic bath with a mixture of de-ionized water and trichloroethylene (TCE) and then washed with boiled acetone. After deposition, ZnO thin films were irradiated with 100 MeV Ag ions (charge state +7) using the 15UD Pelletron accelerator facility at the Inter-University Accelerator Centre (IUAC), New Delhi in Materials Science beam line. The vacuum in a chamber during the irradiation was $\sim 6 \times 10^{-7}$ mbar. The electronic (S_e) and nuclear (S_n) energy losses for 100 MeV Ag ions in ZnO thin film were ~ 20.39 keV//nm and ~ 0.122 keV/nm, respectively and the range of Ag ions in ZnO film was ~ 12.15 μm as calculated by Stopping and Range of Ions in Matter (SRIM) simulation programme. The ion beam was scanned over an area of 1×1 cm^2 with fluence 3×10^{12}, 1×10^{13} and 3×10^{13} ions/cm^2 and the beam current was kept constant at 1 pnA (particle nanoampere).

The phase formation and crystal structure of the films before as well as after irradiation were studied by Bruker X-ray diffractometer with CuK_α ($\lambda = 1.54$ Å) monochromatic radiation source. The UV–visible transmission spectra of pristine and irradiated thin films were measured by the dual beam U-3300 Hitachi Spectrometer at Inter-University Accelerator Centre (IUAC), New Delhi. The surface topography was observed by atomic force microscopy (Bruker) and scanning electron microscopy (Nova Nano FE-SEM 450 FEI). Micro-Raman spectra of pristine and irradiated ZnO thin films were obtained by using Renishaw in-Via micro-Raman microscope with Ar ion laser excitation wavelength at 514.5 nm with 10 mW power.

3. Results and discussion

3.1. XRD measurements

The structural behaviour of ZnO thin films is investigated using X-ray diffraction (XRD) pattern. Fig. 2 shows the XRD pattern for pristine, and 100 MeV Ag^{7+} ions irradiated films at the different ion fluence 3×10^{12}, 1×10^{13}, and 3×10^{13} ions/cm^2. The XRD pattern of pristine film confirm the presence of crystalline hexagonal wurtzite structure with reflection from (100), (002), and (101) planes at ~31.7°, 34.4°, and 36.2° respectively (JCPDS Card No. 89-1397). After the irradiation, the intensity of the reflections corresponding to (100) and (101) planes is observed to be decreased when the incident fluences increased. Whereas, at the highest fluence (3×10^{13} ions/cm^2) the intensity corresponding to (002) plane is found to be increased drastically with increased fluences which is indicating the growth of the grain along the c-axis. On the other hand, the peaks associated with (100) and (101) planes are almost vanished at this highest fluence (shown in Fig. 2). The increased intensity is indicating the improved crystallinity of ZnO films. It is observed that at the higher fluences, film releases strain, which is responsible for growth in *c*-axis orientation because (002) plane of ZnO is having the lowest surface energy according to basic crystal growth theory [34, 35]. The strain can be estimated by using the following relation [36]:

$$\varepsilon = \frac{\beta Cos\theta}{4Sin\theta} \quad (1)$$

where, β is full width at half maximum (FWHM) in radian and θ is the angle of diffraction. The size of ZnO crystallite is calculated using the following Debye–Scherrer's formula [37]:

$$D = \frac{0.9\lambda}{\beta cos\theta} \quad (2)$$

In Eq. (2), λ, β, and θ are X-ray wavelength ($CuK_\alpha = 1.54$ Å), FWHM and the Bragg diffraction angle, respectively. The calculated average crystallite size (Fig. 3) of the pristine ZnO film is 10.8 ± 0.7 nm which is increased up to 20.5 ± 0.3 nm with increasing the ion fluences and summarized in Table 1. During swift heavy ion irradiation, the thermal spike model is the dominant mechanism for all the structural modifications according to which incident ions transfer a large amount of energy into the target material due to electronic energy loss (S_e). This large amount of energy creates the very high-temperature zones in the target material, which is responsible for the structural modifications. In this process, film releases the strain at higher fluence leads to the crystalline behaviour of the film [38]. The increased crystallinity along the preferred c-axis orientation of ZnO thin film could be suitable for piezoelectric transduction mechanism [39].

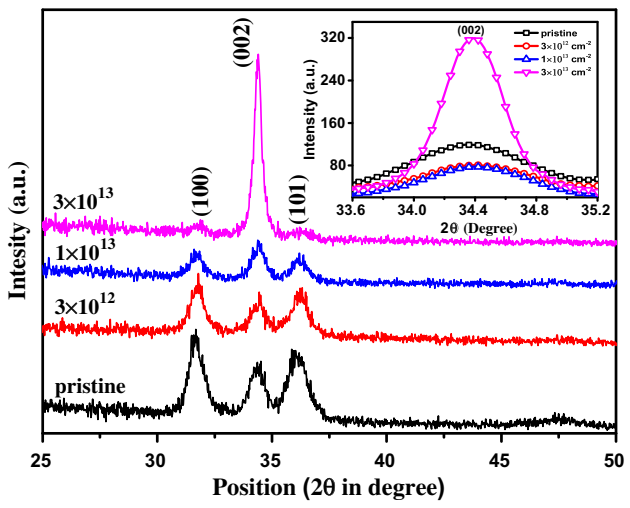

Fig. 2 XRD spectra of the pristine and irradiated ZnO thin films with different fluences. *Inset* shows the zoomed behaviour of (002) plane with ion irradiation

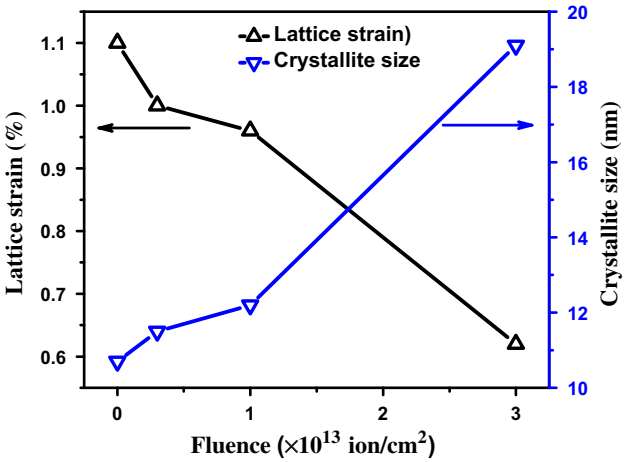

Fig. 3 Variation of the lattice strain and crystallite size with different ion fluences

Table 1 Variation of crystallite size with different ion irradiation fluences

Fluences (ions/cm^2) 100 MeV Ag ions	Crystallite size (in nm) with error
Pristine	10.8 ± 0.7
3×10^{12}	12.6 ± 0.9
1×10^{13}	12.7 ± 0.6
3×10^{13}	20.5 ± 0.3

3.2. UV–visible spectroscopy

Optical properties of pristine and irradiated ZnO thin films are analysed by UV–visible spectroscopy. The transmission spectra in the visible region of the electromagnetic spectrum of ZnO thin films are shown in Fig. 4. It is observed from spectra that there is a significant change in transmittance of ZnO thin films with increasing ion fluences. The transmittance of the pristine and irradiated film at higher fluence 3×10^{13} ions/cm^2 are found to be ~90 and 80% respectively at 550 nm. The reduction in transmittance of the film at higher fluence is attributed to the increased electron carrier density and defect creation such as oxygen vacancies induced by SHI irradiation in ZnO thin film [40]. ZnO is a direct band gap material, and the band gap of the pristine and irradiated ZnO thin films is determined using Tauc's relation [41] which is expressed as

$$\alpha h\upsilon = A\left(h\upsilon - E_g\right)^{1/n} \tag{3}$$

In Eq. (3), α is the absorption coefficient, hυ is the incident photon energy, E_g is the optical band gap, and A is constant. The index value "n" depends on the transition whether it is direct or indirect and allowed or forbidden. For the direct band gap, the value of n = 2. The band gap value is calculated by extrapolating the linear part of the spectra of $(\alpha h\upsilon)^2$ versus hυ plot (inset). It is observed that the band gap of the ZnO films is slightly increased (from 3.28 to 3.30 eV) with ion irradiation. The variation in band gap can be explained by Burstein–Moss effect (B–M effect) which depends on electron carrier concentration in the material which affected by SHI irradiation [42].

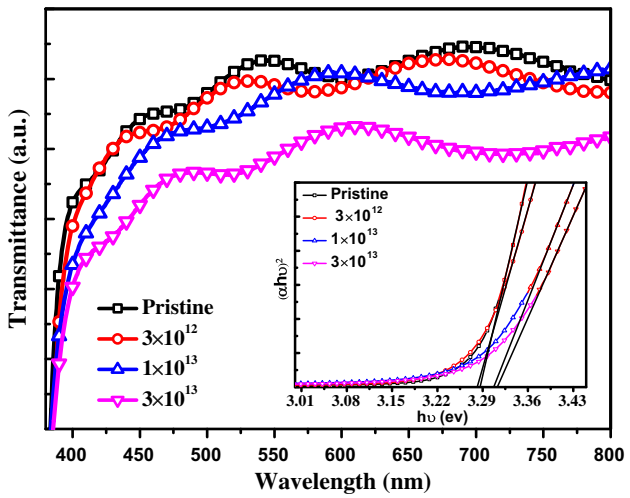

Fig. 4 UV–visible transmission spectra for pristine and 100 MeV Ag ion irradiated films of ZnO. Band gap variation of pristine and irradiated film calculated by Tau'c plot (*inset*)

3.3. Atomic force microscopy

The surface morphology of pristine and irradiated ZnO thin films is observed by AFM in tapping mode. Fig. 5 shows the three-dimensional (5×5 μm^2) micrographs of pristine and 100 MeV Ag^{7+} irradiated ZnO thin films. It is clear from the images that ZnO grains are connected to each other and films are grown uniformly on the substrate. Fig. 6 shows the Gaussian distribution of grain size of the pristine and irradiated ZnO thin films at different fluences. The grain size of the thin films is increased with increasing the ion fluence which is associated to the agglomeration of the ZnO grains with ion irradiation. The calculated grain size of the pristine film is around to be ~198 ± 6.8 nm, and it increases up to ~219 ± 2.8 nm at the fluence of 3×10^{13} ion/cm^2. The discrimination in the calculated grain size from AFM and XRD is observed because XRD pattern determines the average crystallite size whereas the AFM shows the agglomeration of particles at the surface, which are much bigger than those observed by XRD. The observations of AFM and XRD can be correlated by the fact that smaller particles have a larger surface free energy, therefore, agglomerate faster and develop larger grains and XRD is related to smaller particles whereas AFM gives larger grains [43]. The root-mean-square roughness (R_{rms}) of the pristine and irradiated films is calculated using following relation [32];

$$R_{rms} = \left[\frac{1}{N}\sum_{i=1}^{N}|Z_i - \overline{Z}|^2\right]^{1/2} \tag{4}$$

where N is a number of surface height data, and Z is the mean height distance. The estimated roughness of the pristine ZnO films is 10.2 nm and varied marginally with incident fluences shown in Fig. 7. The variation in grain size and roughness of the film have been summarized in Table 2. When swift heavy ions pass through the material, transfers a large amount of energy into the material. If the surface energy of the film is greater than acquired energy from incident ions, then it leads to agglomeration of the grains and formed the bigger grains due to surface diffusion process near the top surface of the thin film. With the increase of ion fluences, the surface energy of the film changes due to total energy ($S_e \times \phi$) deposited by incident ions. This surface diffusion process is responsible for the

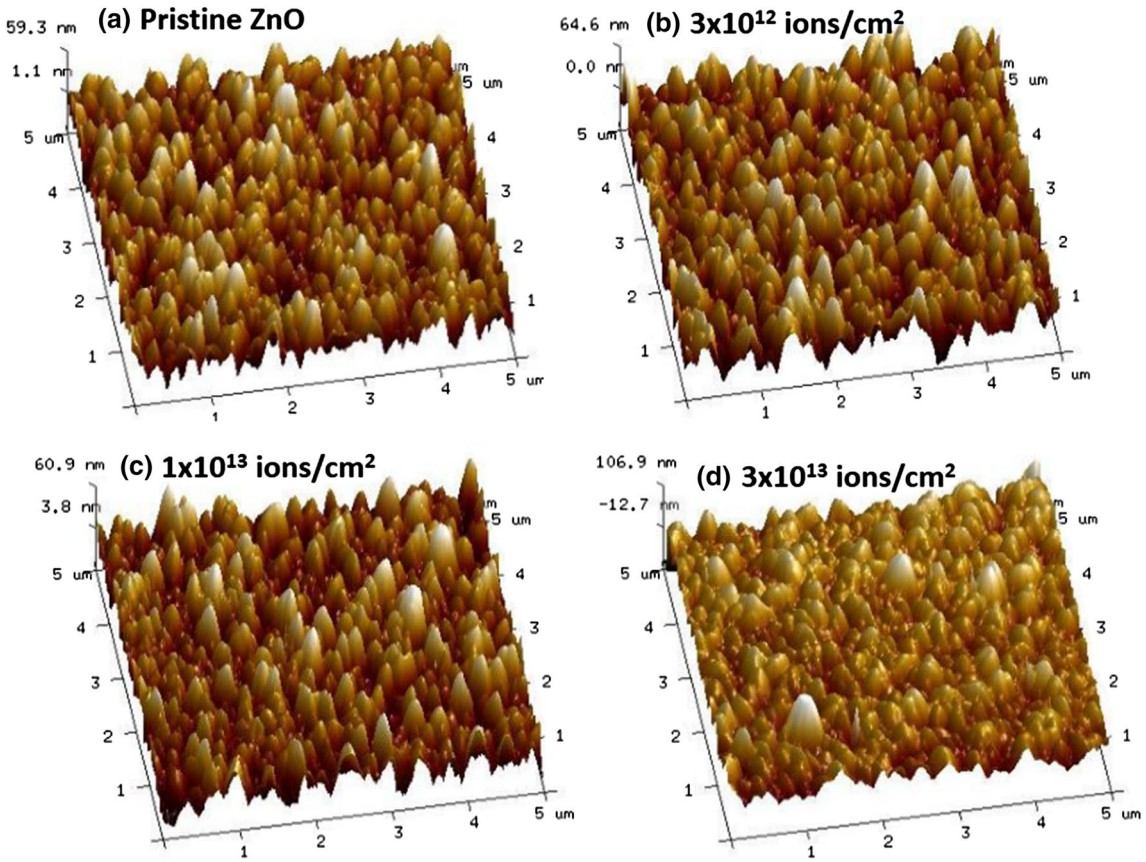

Fig. 5 AFM micrographs of (**a**) Pristine (**b**) 3×10^{12} ion/cm^2 (**c**) 1×10^{13} ion/cm^2 and (**d**) 3×10^{13} ion/cm^2

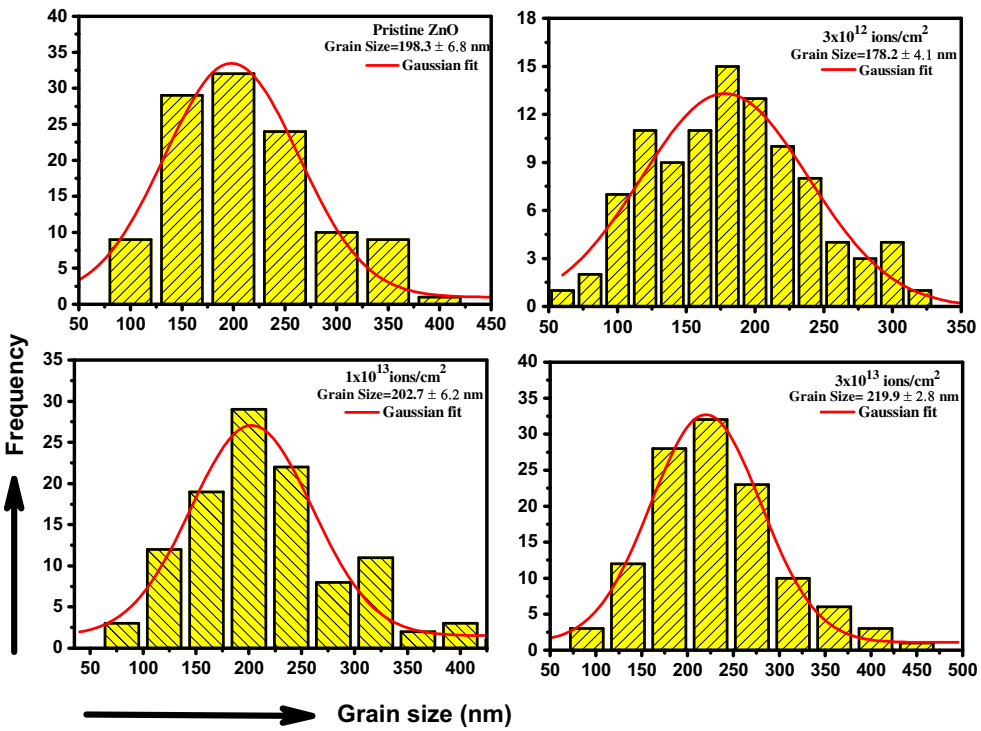

Fig. 6 Variation of grain size with different ion fluences calculated by atomic force microscopy

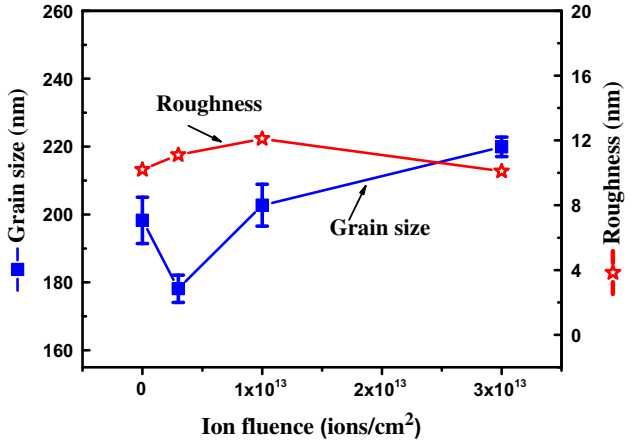

Fig. 7 Variation of roughness and grain size with different ion irradiation fluences

Table 2 Grain size and roughness of the film with different fluences

Fluence (ions/cm^2) 100 MeV Ag ions	Grain size (nm) with error	Roughness (nm)
Pristine	198.3 ± 6.8	10.2
3×10^{12}	178.2 ± 4.1	11.1
1×10^{13}	202.7 ± 6.2	12.1
3×10^{13}	219.9 ± 2.8	10.1

grain growth and change in shape and size of the grains near surface region [31].

3.4. Field emission scanning electron microscopy

Figure 8(a)–(d) shows the FESEM micrographs of the pristine and irradiated films at fluence of 3×10^{12}, 1×10^{13} and 3×10^{13} ions/cm^2. The thin film irradiated at higher fluence (3×10^{13} ions/cm^2) is showing the agglomeration of the particles over the surface (Fig. 8(d)) which is further supported the AFM study. Agglomeration of ZnO particles in the film increases with increasing the ion fluence, which is attributed to rising the local melting temperature on the surface due to the interaction of high energetic ions. FESEM results are showing larger grains with different size and shape on the top surface of the film. The agglomeration of the particles is also observed in SEM images at the higher fluence which has already mentioned above in AFM analysis.

3.5. Micro-Raman spectroscopy

The Raman active phonon modes of the wurtzite structure of ZnO as expected from the group theory are $A_1 + 2E_2 + E_1$ modes, where all atoms occupy C_{3v} sites [44, 45]. Typical micro-Raman spectra of the ZnO thin films irradiated with fluences 3×10^{12}, 1×10^{13} and 3×10^{13} ions/cm^2 are shown in Fig. 9. The spectra confirm the presence of the peaks at 280, 440 cm^{-1}, very sharp peak at 573 cm^{-1}, broad peak at 630 and 780 cm^{-1} for the pristine as well irradiated ZnO thin films. The weak Raman mode B_1 (high) − B_2 (low) and B_1 (high) + B_1 (low) are recorded at 280 and 780 cm^{-1}. The peak at 573 cm^{-1} can be assigned to A_1 (LO) mode, which is in good agreement with the theoretical calculations [46]. Small band at 630 cm^{-1} is assigned to the E_1 (LO) mode [47]. The B_1 (high) − B_2 (low) and B_1 (high) + B_1 (low) modes are not much affected by SHI irradiation. The intensity of the peak at 573 cm^{-1} decreases slowly with the increase the ion fluences, while E_2 (high) mode at 440 cm^{-1} decreases at the fluence of 3×10^{13} ions/cm^2. The characteristic modes of ZnO, E_2 (high) and A_1 (LO) at 440 and 573 cm^{-1} respectively are associated to the highly textured and wurtzite structure of the ZnO thin film (inset). The pristine ZnO thin film seems to be oxygen deficient as indicated by the A_1 (LO) mode at 573 cm^{-1} with higher intensity. Swift heavy ion induced density of defects and disorder is subjected to loss of the translation symmetry of the lattice of the material, which leads to the invalidations of the $k = 0$ wave vector selection rule from all part of the Brillouin zone in Raman scattering. Therefore Irradiation-induced A_1 (LO) mode is explained in the term of surface phonon mode which is directly related to intrinsic lattice defects in the material structure. Other Raman modes of the ZnO thin film have been related to the formation of wurtzite structure of the ZnO according to the selection rule [32].

The decrement in the intensity corresponding to (100) and (101) planes with increasing fluence and enhanced *c*-axis orientation of ZnO thin films along the (002) plane at the highest fluence are observed. The improvement in crystallinity can be described in light of interaction of ion and materials. The imparted energy from the incident high energy ions to target material is responsible for the electronic ionizations/excitations and lattice vibrations along the ion path. These vibrations and excitations cause to the releases of strain in the film which lowers the surface energy. Therefore, ZnO thin film become oriented along (002) plane as it has lower surface energy and resulted in increased crystallinity after irradiation. Raman spectra confirm the formation of wurtzite structure of ZnO films. In the present study the observed A_1 (LO) mode at 573 cm^{-1} is related to the intrinsic lattice defects in the ZnO structure. The decrease in the intensity of A_1 (LO) mode further confirms the increase lattice defects in the ZnO film due to high energetic ions. These ion-induced defects and vacancies play a major role to tune the optical properties of ZnO thin films. The reduction of transmittance at higher fluence attributed to the increased electron carrier density and defect creation such as oxygen vacancies induced by

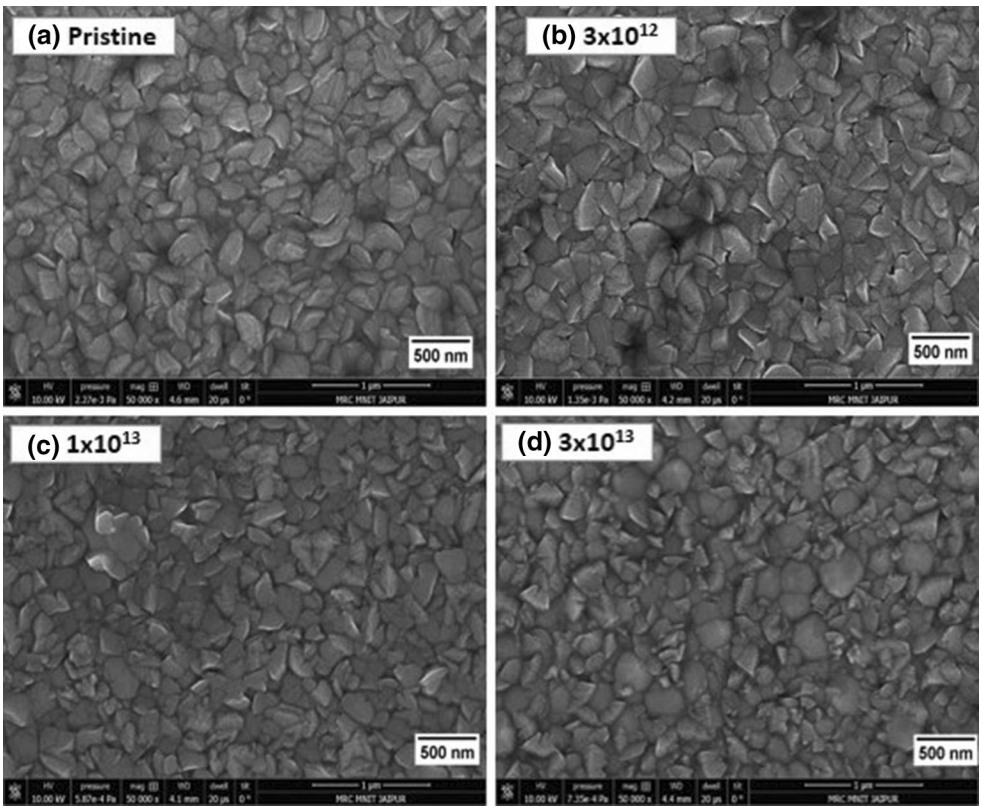

Fig. 8 FESEM micrographs of pristine and 100 MeV Ag ion irradiated film of ZnO at different fluences

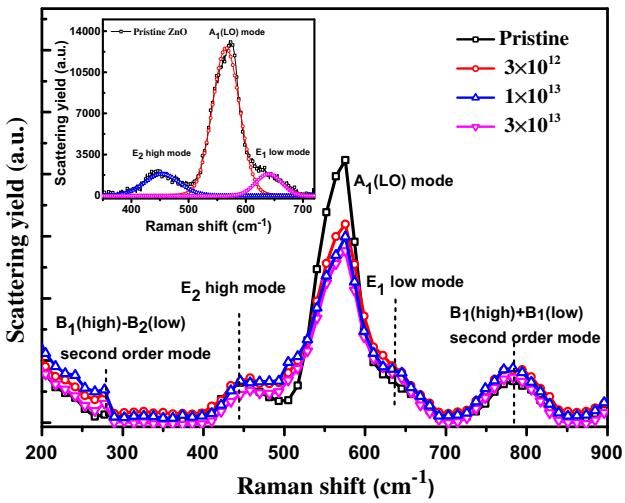

Fig. 9 Raman spectra of pristine and 100 MeV Ag irradiated at different fluences

SHI irradiation in ZnO thin film. The band gap is also slightly increased (from 3.28 to 3.30 eV) with ion irradiation and it might be attributed to electron carrier concentration which can be explained in the term of Burstein-Moss effect (B-M effect). These modifications in the films are subjected to change in surface energy of the films which is also responsible for grain growth and morphological features of the film with ion irradiation. Therefore such kind of ZnO thin film can be used in radiation harsh environment and optoelectronic applications.

4. Conclusions

In summary, the structural, optical and morphological modifications of ZnO thin films are investigated by using SHI irradiation. The enhancement in the crystallinity along the c-axis orientation due to the impact of energetic ions is confirmed by XRD analysis. It is observed that optical properties can be tailored by ion irradiation as transmittance decreases with higher irradiation fluence. This property can be used in transparent window materials. The dependence of surface morphology and grain size on incident ions are further confirmed by AFM and FESEM analysis and observed the increased grain size after irradiation. All the induced modifications are explained in terms of energy loss of ions into the target materials.

Acknowledgements One of the authors (Shushant Kumar Singh) is thankful to the Technical Education Quality Improvement Programme (TEQIP), MNIT Jaipur for providing the financial assistantship. The authors would like to thank Inter-University Accelerator Centre (IUAC) New Delhi for providing the necessary synthesis and

experimental facilities and highly grateful to pelletron group for providing the stable beam during swift heavy ion irradiation experiment. The authors are also thankful to the Materials Research Centre, MNIT Jaipur for providing characterization techniques (AFM and FESEM). One of the authors (R. Singhal) highly acknowledges the financial support provided by DST New Delhi DST FAST young scientist Project (SR/FTP/PS-081/2011), DST INSPIRE Faculty Project (IFA11PH-01) and UGC New Delhi (P.F. No. DRC-14/59/2013/10/169/00036). R. Vishnoi is greatly thankful to DST New Delhi for financial help under DST FAST Young Scientist Project (SR/FTP/PS-029/2012).

References

[1] C S Chen, C T Kuo, T B Wu and I N Lin, *J. Appl. Phys.* **36,** 1169 (1997)
[2] J M Hvam *Phys. Rev. B,* **4,** 4459 (1971)
[3] J H Lee, K H Ko and B.D. Park, *J. Cryst. Growth,* **247,** 119 (2003)
[4] M M Bagheri-Mohagheghi and M Shokooh-Saremi, *Thin Solid Films,* **441,** 238 (2003)
[5] J Hu and R G Gordon, *J. Appl. Phys.* **71,** 238 (1992)
[6] X W Sun and H S Kwok, *J. Appl. Phys.* **86,** 408 (1999)
[7] D C Agarwal *et al. Surf. Coat. Technol.* **203,** 2427 (2009)
[8] J F Wager, *Science,* **300,** 1245 (2003)
[9] S J Pearton, D P Norton, K Ip, Y W Heo and T Steiner, *Prog. Mater. Sci.* **50,** 293 (2005)
[10] M J Gratzel, *Photochem. Photobiol. A,* **3,** 164 (2004)
[11] P F Carcia, R S Melean, M H Reilly and G Nunes, *Appl. Phys. Lett.* **82,** 1117 (2003)
[12] D C Look, D C Reynolds, C W Letton, R L Jones, D B Eason and G Cantwell, *Appl. Phys. Lett.* **81,** 1830 (2002)
[13] T Gao and T H Wang, *Appl. Phys. A,* **80,** 1451 (2005)
[14] Z W Pang, Z R Dai and Z L Wang, *Science,* **291,** 1947 (2001)
[15] M H Huang, Y Y Wu, H Feick, N Tran, E Weber and P D Yang, *Science,* **292,** 1897 (2001)
[16] C H Liu, W C Yiu, F C K Au, J K Ding, C S Lee and S T Lee, *Appl. Phys. Lett.* **83,** 3168 (2003)
[17] P Shah, S Kumar, A Gupta, R Thangaraj and D K Avasthi, *Nucl. Instrum. Methods Phys. Res. B,* **156,** 222 (1999)
[18] R Singhal *et al. J. Phys. D: Appl. Phys.* **42,** 155103 (2009)
[19] R Singhal, A Kumar, Y K Mishra, S Mohapatra, J C Pivin and D K Avasthi, *Nucl. Instrum. Methods B,* **266,** 3257 (2008)
[20] R Vishnoi, R Singhal, K Asokan, D Kanjilal and D Kaur, *Thin Solid Films,* **520,** 1631 (2011)
[21] R Singhal, D Kabiraj, P K Kulriya, J C Pivin, R Chandra and D K Avasthi, *Plasmonics,* **8,** 295 (2013)
[22] R Singhal, J C Pivin and D K Avasthi, *J. Nanopart. Res.* **15,** 1641 (2013)
[23] D K Avasthi, Y K Mishra, F Singh and J P Stoquert, *Nucl. Instr. Meth. B,* **268,** 3027 (2010)
[24] Y K Mishra *et al. Nucl. Instrum. Methods B,* **266,** 1804 (2008)
[25] V Kumar, F Singh, O M Ntwaeaborwa and H.C. Swart, *Appl. Surf. Sci.,* **279,** 472 (2013)
[26] S Kumar, R Kumar and D P Singh, *Appl. Surf. Sci.,* **255,** 8014 (2009)
[27] D K Avasthi, A Kumar, R Singhal, A Tripathi and D S Mishra, *J. Nanosci. Nanotechnol.* **10,** 3767 (2010)
[28] D K Avasthi and G K Mehta, *Swift heavy ions for materials engineering and nanostructuring*, Springer, Netherland (2011)
[29] S K Srivastava *et al. Phy. Rev. B,* **71,** 193405 (2005)
[30] W Bolse and B Schattat, *Nucl. Instrum. Methods Phys. Res. B,* **190,** 173 (2002)
[31] D C Agrawal, R S Chauhan, D K Avasthi, S A Khan, D Kabiraj and I Sulaniya, *J. Appl. Phys.* **104,** 024304 (2008)
[32] F Singh, R G Singh, V Singh, S A Khan and J C Pivin, *J. Appl. Phys.* **110,** 083520 (2011)
[33] S Rehman, R G Singh, J C Pivin, Waseem Bari and F Singh, *Vacuum,* **86,** 87 (2011)
[34] N Fujimura, T Nishinara, S Goto, J Xu and T Ito, *J. Cryst. Growth,* **130,** 269 (1993)
[35] A N Mariano and R E Hanneman, *J. Appl. Phys.* **34,** 384 (1963)
[36] H P Klug and L E Alexander, *X-ray Diffraction Procedures for Polycrystalline and Amorphous Materials*. Wiley, New York (1974)
[37] B D Cullity, *Elements of X-ray diffraction*, *Addison-Wesley*, Reading (1970)
[38] G. Szenes, *Phys. Rev. B,* **51,** 8026 (1995)
[39] J G E Gardeniers, Z M Rittersma and G J Burger, *J. Appl. Phys.* **83,** 12 (1998)
[40] P M R Kumar *et al. J. Appl. Phys.,* **97,** 013509 (2005)
[41] J Tauc, *Mater. Res. Bull.,* **3,** 37 (1968)
[42] Marius Grundmann, *The Physics of Semiconductors*, *New York: Springer* (2006)
[43] R Vishnoi and D Kaur, *Surf. Coat. Technol*., **204,** 3773 (2010)
[44] J F Scott, *Phys. Rev. B,* **2,** 1209 (1970)
[45] C Bundesmann *et al. Appl. Phys. Lett*. **83,** 1974 (2003)
[46] V A Fonoberov and A A Balandin, *Phys. Rev. B,* **70,** 233205 (2004)
[47] A Zaoui and W Sekkal, *Phys. Rev. B,* **66,** 174106 (2002)